



PCCP

**Quantum and Semiclassical Studies of Nonadiabatic
Electronic Transitions between N(4S) and N(2D) by
Collisions with N₂**

Journal:	<i>Physical Chemistry Chemical Physics</i>
Manuscript ID	CP-ART-03-2023-001429.R1
Article Type:	Paper
Date Submitted by the Author:	12-May-2023
Complete List of Authors:	Lu, Dandan; University of New Mexico College of Arts and Sciences, Department of Chemistry and Chemical Biology Galvão, Breno; Centro Federal de Educação Tecnológica de Minas Gerais, CEFET-MG, Departamento de Química Varandas, Antonio; Qufu Normal University; Universidade de Coimbra, Guo, Hua; University of New Mexico College of Arts and Sciences, Department of Chemistry and Chemical Biology

SCHOLARONE™
Manuscripts

Submitted to PCCP, 3/28/2023, revised 5/12/2023

**Quantum and Semiclassical Studies of Nonadiabatic Electronic Transitions
between N(⁴S) and N(²D) by Collisions with N₂**

Dandan Lu,¹ Breno R. L. Galvão,² Antonio J. C. Varandas,^{3,4} and Hua Guo^{1,*}

¹*Department of Chemistry and Chemical Biology, University of New Mexico,*

Albuquerque, New Mexico 87131

²*Centro Federal de Educação Tecnológica de Minas Gerais, CEFET-MG, Av.*

Amazonas 5253, (30421-169), Belo Horizonte, Minas Gerais, Brazil

³*Departamento de Física, Universidade Federal do Espírito Santo, Vitória, Brazil*

⁴*Coimbra Chemistry Centre and Chemistry Department, University of Coimbra,*

Coimbra, Portugal

*: corresponding author: hguo@unm.edu

Abstract

The dynamics and kinetics of spin-forbidden transitions between N(²D) and N(⁴S) via collisions with N₂ molecules are investigated using a quantum wave packet (WP) method and the semi-classical coherent switches with decay of mixing (CSDM) method. These electronic transition processes are competing with exchange reaction channels on both the doublet and quartet potential energy surfaces. The WP and CSDM quenching rate coefficients are found in reasonable agreement with each other, and both

reproduce the previous theoretical results. For the excitation process, the agreement between the two approaches is dependent on the treatment of the zero-point energy (ZPE) in the product, because the high endoergicity of this process leads to severe violation of the vibrational ZPE. The Gaussian-binning (GB) method is found to improve the agreement with the quantum result. The excitation rate coefficients are found to be two orders of magnitude smaller than that of the adiabatic exchange reaction, underscoring the inefficient intersystem crossing due to the weak spin-orbit coupling between the two spin manifolds of the N_3 system.

I. Introduction

The two lowest-lying states of atomic nitrogen, $N(^4S)$ and $N(^2D)$, are separated by an energy gap of 2.38 eV. While the ground state $N(^4S)$ typically reacts with a significant barrier, the excited state $N(^2D)$ is often involved in barrierless reactions.¹⁻³ This difference in reactivity has significant implications in modeling gas phase chemistry of extreme environments, such as Earth's ionosphere,⁴ combustion,⁵ and the boundary layer of a hypersonic entry vehicle.^{6, 7} To this end, a detailed understanding of the collisional induced quenching and excitation processes of atomic nitrogen is highly desired. In Earth's atmosphere, the collision partner is likely N_2 . As a result, the following quenching (R1):



and the reverse excitation (R-1) processes are of great importance.

Most experimental studies have so far been restricted to the quenching rate of $N(^2D)$ by collisions with N_2 , namely R1, at relatively low (~ 300 K) temperatures.⁸⁻¹⁵ Theoretically, many ab initio calculations have been carried out, in particular related to the elusive N_3 species,¹⁶⁻¹⁸ which is a candidate for high energy-density materials.¹⁹ For understanding collisional processes, global potential energy surfaces (PESs) are needed. The earlier empirical PESs²⁰⁻²² have now been displaced by more accurate ab initio-based ones for both the doublet and quartet states.²²⁻²⁸ The availability of these PESs have enabled quantum and classical studies of the adiabatic reactive and elastic scattering between N and N_2 .^{23, 27, 29-34}

The $N(^2D) + N_2$ asymptote correlates with five doublet states, while the $N(^4S) + N_2$ asymptote correlates with one quartet state. The quenching and excitation processes are intrinsically non-Born-Oppenheimer, as the transitions are induced by spin-orbit coupling between the doublet and quartet spin manifolds. Hence, a dynamical study of the nonadiabatic dynamics requires not only knowledge of PESs in the two spin manifolds, but also their coupling. Accurate doublet and quartet PESs have recently been developed by Galvão et al.,²⁶⁻²⁸ and approximate spin-orbit couplings have also been determined by Zhang et al.¹⁸

Ideally, a fully quantum mechanical characterization is needed for an accurate characterization of nonadiabatic dynamics.³⁵⁻³⁷ However, such a treatment is numerically expensive, even for triatomic systems, so approximations are often necessary. To this end, the most popular approach for treating nonadiabatic transitions

is the Trajectory Surface Hopping (TSH) method,³⁸ in which the electronic coordinates are treated quantum mechanically while the nuclear coordinates classically. However, the modern version of TSH, namely so-called Fewest Switches Surface Hopping (FSSH) method,³⁹ sometimes suffers from overestimation of electronic coherence.⁴⁰ Many improvements over the FSSH method have been proposed,⁴¹⁻⁴³ but we will in this work use the Coherent Switching with Decay of Mixing (CSDM),⁴⁴ which has been tested in many systems,⁴⁵ including our recent study of the spin-forbidden excitation of C(³P) to C(¹D) by collisions with N₂.⁴⁶ These semiclassical methods are numerically inexpensive and thus can be used for larger systems. However, it is essential to valid such a semi-classical approach against exact quantum mechanical calculations.

For the current system, Galvão et al.^{47, 48} recently published TSH investigations of the N(²D) quenching (R1) kinetics using the most recent PESs²⁶⁻²⁸ and the agreement with the available experimental rate coefficients was satisfactory, especially given the fact that the experimental data are quite scattered. However, there has been no theoretical study on the excitation process (R-1), which is needed for modelling hyperthermal chemistry. In this publication, we report WP and CSDM results for R1 and R-1 using the same PESs and spin-orbit coupling used by Galvão et al.⁴⁷ We first compare our WP calculations to the earlier TSH results for quenching (R1).⁴⁷ This is followed by new results for excitation (R-1), using both WP and CSDM methods. It is important to point out that the intersystem crossing between the two N+N₂ spin states is inefficient, as the spin-orbit coupling is proportional to atomic number. For this light system, it can be expected that the spin flip is an improbable event, particularly when

other channels are open. This characteristic poses a stringent test of the semi-classical method. In addition, R1 and R-1 are competing with the exchange channel:



which might or might not include electronic transitions:



While R2a is also facilitated by spin-orbit coupling, the adiabatic exchange reaction R2b is controlled by the barrier on the adiabatic PES of the quartet state. Such exchange channels are known to be efficient in hyperthermal collisions.⁴⁹⁻⁵²

In our calculations reported here, R2 is either implicitly included in the WP calculations, through the use of a damping term, or explicitly included in the CSDM calculations. As shown in this work, the adiabatic exchange channel (R2b) has much larger rate coefficients than the nonadiabatic channels (R-1 and R2a). This work is organized as follows. The quantum and semiclassical methods are outlined in Sec. II. The results and discussion are presented in Sec. III. The conclusions are given in Sec. IV.

II. Theory

II-A. Quantum dynamics

The WP scattering calculations were performed in the N-N₂ Jacobi coordinates (R ,

r , θ), in which r is the N-N distance, R the distance between N and N_2 , and θ the angle in between. The corresponding Hamiltonian has the following form ($\hbar=1$):

$$\hat{H} = -\frac{1}{2\mu_R}\frac{\partial^2}{\partial R^2} - \frac{1}{2\mu_r}\frac{\partial^2}{\partial r^2} + \frac{(\vec{J}-\vec{j})^2}{2\mu_R R^2} + \frac{\vec{j}^2}{2\mu_r r^2} + \hat{H}_{el}, \quad (1)$$

where μ_R is the reduced mass between N and N_2 , and μ_r are the reduced mass of N_2 . \vec{J} and \vec{j} are the total and N_2 rotational angular momentum operators, respectively. The electronic Hamiltonian (\hat{H}_{el}) is given in the form of a potential matrix. The details of the N_3 PESs for these two spin manifolds and their spin-orbit couplings have been discuss in Ref. ⁴⁷, and the intersystem crossing can be approximated by a three-state model, which include the $1^2A'$, $1^2A''$ and $1^4A''$ states.⁴⁷

We note here that N_2 has two forms, *para* and *ortho*, depending on its nuclear spin. In an exact treatment, the nuclear spin angular momentum should be coupled with the electronic and rotational angular momenta of the molecule, which complicates the calculations. In this work, the nuclear spin is ignored as an approximation. This is needed to have a meaningful comparison with the semi-classical methods, which cannot distinguish the nuclear spin states.

The WP calculations were performed in the body-fixed (BF) frame using the Chebyshev propagator.⁵³ The initial wave packet in the $N(^2D)/N(^4S) + N_2$ channel associated with an N_2 ro-vibrational state labeled by the corresponding quantum numbers (v_i, j_i) has the following form:

$$\Psi_{v_i j_i}^{JM \varepsilon} = G(R) \phi_{v_i j_i}(r) |JM j_i l_i \varepsilon\rangle, \quad (2)$$

where $|JMj; l_i \varepsilon\rangle$ is the eigenfunction of the total angular momentum in the space-fixed (SF) representation, $\varepsilon = (-1)^{j_i + l_i}$ is parity and $\phi_{v_j i}(r)$ defines the rovibrational eigenfunction for N_2 . l_i is the initial orbital angular momentum ($\vec{l} = \vec{j} - \vec{j}$). M is the projection of J onto the Z axis of the SF frame. $G(R)$ is a Gaussian wave packet along the scattering coordinate defined as

$$G(R) = N \exp \left[-\frac{(R - R_i)^2}{\tau^2} \right] \cos(k_i R), \quad (3)$$

in which N is the normalization factor, R_i is the initial position of the wave packet, k_i is wave vector, τ is the width of the wave packet in the scattering coordinate.

The discrete Chebyshev propagator is employed in the BF to propagate the wave packet in the order domain of the propagator (k) as follows:⁵⁴

$$\Psi_{k+1} = 2D\hat{H}_{scaled}\Psi_k - D^2\Psi_{k-1}, \quad (k > 1) \quad (4)$$

with $\Psi_1 = 2D\hat{H}_{scaled}\Psi_0$. To avoid divergence of the Chebyshev operator, the Hamiltonian is scaled: $\hat{H}_{scaled} = a_s\hat{H} - b_s$, where $a_s = \frac{2}{H_{max} - H_{min}}$, $b_s = 1 + a_s H_{min}$.⁵⁵ The extrema of the Hamiltonian are estimated from the grid/basis used in the calculation. The Chebyshev propagator is more efficient and accurate than the time propagator because the latter requires interpolation.^{53, 56} Finally, D is the damping function that prevents reflection at the edge of the grid. For the R grid:

$$D_R = \exp \left(-0.01 \Delta_t \left[\frac{R - 13.07}{5.00} \right]^2 \right), \quad 13 < R < 18 \text{ bohr} \quad (5)$$

with parameters listed in Table 1. The parameter $\Delta_t = \frac{a_s}{\sqrt{1 - [(E_{v_j i} + E_i) * a_s - b_s]^2}}$ is defined

in Ref. ⁵⁷, E_{vji} is the initial rovibrational energy, E_i is the collision energy of the initial wave packet. Similar damping terms are placed in the r grid edge:

$$D_r = \begin{cases} \exp(-0.005\Delta_t \left[\frac{r-6.0}{0.8} \right]), & 6.0 < r < 6.8 \text{ bohr} \\ \exp(-0.003\Delta_t \left[\frac{r-5.0}{1} \right]), & 5.0 < r < 6.0 \text{ bohr} \end{cases} \quad (6)$$

This prevents the reflection from the exchange channel. Tests are performed to demonstrate that quenching/excitation probabilities are converged with the parameters in Eq. (6).

In the end of the propagation, the BF scattering wave function was transformed into the SF representation, then the desired state-to-state scattering matrix elements, $S_{v_j j_f l_f \leftarrow v_j i l_i}^{\varepsilon}$ in the SF representation can be extracted from imposing the asymptotic boundary conditions. Finally, the state-to-state integral cross-section (ICS) as a function of the collision energy ($E_c = E - \varepsilon_{v_j i}$) is given as follows:

$$\sigma_{v_j j_f l_f \leftarrow v_j i l_i}(E_c) = \frac{1}{(2j_i + 1)2\mu_R E_c} \sum_{j\varepsilon} \sum_{l_f} \sum_{l_i} (2J + 1) P_{v_j j_f l_f \leftarrow v_j i l_i}^{\varepsilon}(E_c) \quad (7)$$

with the state-to-state probabilities

$$P_{v_j j_f l_f \leftarrow v_j i l_i}^{\varepsilon}(E_c) = |S_{v_j j_f l_f \leftarrow v_j i l_i}^{\varepsilon}(E_c)|^2. \quad (8)$$

The initial state specified rate coefficient as a function of the temperature (T) in Kelvin can be respectively calculated by:

$$k_{v_j i}(T) = g_e(T) \sqrt{\frac{8k_B T}{\pi\mu_R}} \frac{1}{(k_B T)^2} \sum_{v_j j_f} \int_0^\infty dE_c E_c \exp(-E_c/k_B T) \sigma_{v_j j_f \leftarrow v_j i}(E_c), \quad (9)$$

where k_B is the Boltzmann constant. The partition functions for the reactants are given

below:

$$g_e(T) = q_{R1}/q_{N(^2D)}q_{N_2} \text{ for R1} \quad (10a)$$

$$g_e(T) = q_{R-1}/q_{N(^4S)}q_{N_2}, \text{ for R-1} \quad (10b)$$

where $q_{R1} = 2$, $q_{N(^2D)} = 6 + 4 \exp\left(-\frac{12.53K}{T}\right)$, $q_{N_2} = 1$, $q_{N(^4S)}=4$, $q_{R-1} = 4$. For nonadiabatic transitions, the total rate is the sum of the contributions from the two doublet states ($1^2A'$, $1^2A''$).

As shown in Eq. (9), the ICS is obtained by summing over the reaction probabilities over all partial waves, which are numerically expensive to compute. In this work, we use the standard J -shift approximation⁵⁸ to estimates the $J \neq 0$ partial wave contributions by shifting the explicitly computed probabilities ($J=0$) based on the centrifugal potential at the barrier. Specifically, the rotational constant:

$$B^* = \frac{1}{2\mu_{RR} r^2} \quad (11)$$

is defined at the barrier (4.951 bohr for $^2A''$ and 4.970 bohr for $^2A'$ state) on the doublet PESs. Now we can compute the corresponding results from the J -shifting model. For each J , the probability at collision energy E_c can be approximated by shifting the probability associated with $J_0 (=0)$,

$$P^J(E_c) = P^{J_0}(E_c - (B^* J(J + 1))). \quad (12)$$

Within the J -shifting model, Eq. (9) can thus be replaced by the initial state specified rate coefficient obtained as follows:

$$k_{v_j i}(T) = g_e(T) \sqrt{\frac{2\pi}{(\mu k_B T)^3}} Q_{v_j i}^{J_0}(T) \sum_J (2J+1) e^{-BJ(J+1)/k_B T}. \quad (13)$$

where $Q_{v_j i}^{J_0}(T) = \sum_{v_f j_f} \int P_{v_f j_f l_f \leftarrow v_j i l_i}^{J_0 \varepsilon}(E_c) e^{-E_c/k_B T} dE_c$.

II-B. Semi-classical dynamics

We also used the semiclassical coherent switching with decay of mixing (CSDM) method⁴⁴ for treating nonadiabatic transitions. The CSDM method was designed to mitigate the overcoherence problem in FSSH by damping the electronic coherence. The method has been implemented in the ANT (Adiabatic and Nonadiabatic Trajectories) program,⁵⁹ which was used in the current study. The semiclassical calculations were carried out in the diabatic representation.

To compare with the quantum probability for $J=0$, the initial state of N_2 was specified by $v_i=0,1$, $j_i=0$ in the semiclassical trajectory calculations and the impact parameter (b) was fixed at 0. The initial separation between the collision partners was 9 Å, and a trajectory is terminated when the two were separated again by 9 Å. The probability $P(E_c)$ is given by:

$$P(E_c) = N_p/N_{total}, \quad (14)$$

where N_p and N_{total} are the number of trajectories entered the product (p) channel and the total number of trajectories. The statistical error is determined by $\Delta = \sqrt{(N_{total} - N_p)/N_p N_{total}}$. In these calculations, 50,000 trajectories were used at each energy.

The thermal rate constants were also calculated directly using CSDM method, In these calculations, the initial ro-vibrational state of N_2 and the collision energy was specified by Boltzmann sampling at the target temperature, and the impact parameter (b) was sampled from a uniformly distributed random number $\zeta \in [0,1]$, according to $b = b_{\max}\zeta^{1/2}$, where b_{\max} equal to the initial reactant separation between the collision partners (9 Å). This choice of b_{\max} was tested and found to be sufficient to converge the results.

The thermal rate coefficient was calculated as follows:

$$k(T) = g_e(T) \sqrt{\frac{8k_B T}{\pi \mu_R}} \pi b_{\max}^2 N_p / N_{total}, \quad (15)$$

in which the electronic partition functions are defined the same way as in the quantum calculations. At each temperature, 2,000,000 trajectories were calculated.

Trajectory based methods do not observe quantization. The excitation process is highly endoergic, which might lead to vibrational energy below the zero-point energy (ZPE) of the product. This ZPE-violation is particularly problematic for endoergic processes such as R-1 and R2a. Several approaches have been proposed to mitigate the ZPE-violation in trajectory calculations. One simple approach is to remove ZPE-violating trajectories, which leads to the so-called hard-ZPE approach.⁶⁰ A more reasonable approach is to bin trajectories with a Gaussian weighting function.⁶¹⁻⁶³ In this Gaussian-binning (GB) method, the reaction probability and rate coefficient are computed based on the following equations:

$$P^{GB} = \sum_1^{N_p} G(v_f) / \sum_1^{N_{total}} G(v_f) \quad (16)$$

$$k^{GB}(T) = g_e(T) \sqrt{\frac{8k_B T}{\pi \mu_R}} \pi b_{max}^2 P^{GB} \quad (17)$$

where $G(v_f) = \frac{1}{\pi^{1/2} \epsilon} e^{-(v_f - v_{f0})^2 / \epsilon^2}$. The product vibrational action variable (not integer) and the vibrational quantum number (integer) are denoted as v_f and v_{f0} . The full width at half maximum (FWHM) was set as 0.1 in this work and $\epsilon = \frac{\text{FWHM}}{2\sqrt{\ln 2}}$.

III. Results and Discussion

III A. PESs

The dynamical calculations reported here employed the set of ab initio PESs developed by Galvão et al.²⁶⁻²⁸ For reaction R1 (and R-1), three of the five states available are sufficient, which are the $1^2A'$, $1^2A''$ and $1^4A''$ states. The $1^4A''$ state has been modeled²⁶ to multireference configuration interaction energies including Davidson correction (MRCI(Q))^{64, 65} and also to selected CCSD(T) (coupled-cluster singles and doubles with perturbative correction of triples),⁶⁶ both extrapolated to the complete basis-set limit⁶⁷ and smoothly merged with a scaling process. The $1^2A'$ and $1^2A''$ states were modeled^{27, 28} to MRCI(Q) energies with the AVTZ basis set^{68, 69} (further calculations with the larger AVQZ basis set for this system, have shown to not significantly change the relative energies and were deemed unnecessary²⁷). For all three electronic states, the ab initio energies were fitted to analytical functions following the double many-body expansion (DMBE⁷⁰) method, and mimick all points within chemical precision (root-mean-square deviation within 1.0 kcal mol⁻¹). The rate

constants predicted by this set of PES have been compared to experimental data, and show agreements within the experimental error bars.^{31, 47}

These ab initio PESs form the diagonal elements of a 3×3 diabatic potential energy matrix (DPEM), in which the off-diagonal elements are the spin-orbit couplings of Zhang et al.¹⁸ used in Ref. ⁴⁷. **Figure 1** displays contour plots of the diabatic PESs for the three states in the radial Jacobi coordinates R and r , with θ fixed at 90° (top panel) and 0° (bottom panel). While the quartet PES is largely repulsive, both the $1^2A'$ and $2^2A''$ PESs feature potential wells relative to the $N(^2D) + N_2$ asymptote, also see Figure 2 below. As discussed below, such wells are capable of supporting metastable states that can strongly influence the nonadiabatic dynamics. In addition, both doublet PESs have the same small barriers, 0.12 eV for both the $1^2A''$ and $1^2A'$ states. The solid lines in these panels represent the crossing seam, near which non-adiabatic transitions between the doublet and quartet states take place, facilitated by the spin-orbit coupling. Similar with the $C+N_2$ system,⁴⁶ the crossing seam is mostly parallel to the N-N internuclear distance (r) and perpendicular to the scattering coordinate (R), which suggests that the vibrational excitation in the initial N_2 should have a relatively minor impact and the translational energy along the scattering coordinate might have a significant effect.

To better understand the effect of exchange reaction, R2, which competes with the excitation of atomic nitrogen, **Figure 2** shows contour plots of the three diabatic PESs in the Jacobi radial coordinates R and r , with θ optimized. The relaxation of the angle

variable revealed more clearly the wells in the doublet PESs. The barrier for the adiabatic exchange reaction (R2b) on the quartet PES is 2.00 eV, less than the excitation energy (2.38 eV) of atomic nitrogen, which means that the R2b channel is a strong competitor for the atomic excitation channel. On the doublet PESs, the barrier for exchange is approximately 0.12 eV, as mentioned above.

III B. Quenching of $N(^2D)$

We first examine the quenching of $N(^2D)$ by collision with N_2 (R1). **Figure 3** shows the $J=0$ quantum probability for N_2 initially in its ground rovibrational state. The initial wave packet was launched on both the $^2A'$ and $^2A''$ PESs, and the results are shown in the upper and lower panels. The WP probabilities are small, consistent with the weak spin-orbit coupling. They also contain strong oscillations, due presumably to the numerous metastable resonances supported by the deep wells on the doublet PESs. An interesting observation is an apparent threshold at about 0.1 eV, which can be attributed to the small barrier in both doublet PESs.

To examine the performance of the CSDM method in treating the intersystem crossing, the reaction probabilities calculated at several collision energies using the semi-classical method are shown in **Figure 3** as well. The comparison with the WP results is generally good, with a similar threshold and dependence on the collision energy, but the CSDM probabilities seem to overestimate the WP results somewhat.

We also performed additional WP calculations at $J=20, 40$ and 60 to assess the J -shifting approximation for computing the rate coefficients. In **Figure 4**, the J -shifted

probabilities are compared with the explicitly calculated WP probabilities for these partial waves. For both the $^2A'$ or $^2A''$ states, the J -shift results are in reasonable agreement with explicitly calculated WP probabilities, particularly at low (<0.4 eV) energies, which instills confidence in predicting rate coefficients at low temperatures using the J -shift approximation.

We have computed both quenching rates with and without atom exchange using the CSDM method. **Figure 5** displays the calculated rate coefficients of R1. Since the J -shift results are only reliable at low collision energies, the quantum rate coefficient was only calculated at low temperatures, from 220 to 300 K. For the CSDM case, the rate coefficients for three temperatures, 298, 500 and 1000 K, were calculated. The earlier TSH results of Galvão et al.⁴⁷ were also included in the figure for comparison. These theoretical results are compared with available experimental data,^{9, 11-15} which contain significant uncertainties evidenced by the scattered data points, shown in the inset of the figure.

The quenching of $N(^2D)$ might involve atom exchange, as the energy is typically higher than the exchange barrier on both the doublet and quartet PESs. The quenching with atom exchange can in principle be investigated using different isotopes of nitrogen, but no such experiment has been reported. In **Figure 5**, the total quenching rate coefficient and that without atom exchange are shown and compared with the TSH results reported previously by Galvão et al.⁴⁷ The CSDM results are slightly higher than the TSH results, but have roughly the same slope, suggesting similar activation energies.

The WP rate coefficient has a slightly different slope from the semiclassical counterparts. This somewhat lower activation barrier appears to be due to tunneling. As shown in **Figure 3**, there is a very small but finite probability below the 0.1 eV apparent threshold, which supports the tunneling hypothesis. When these small probabilities were erased, the slope of the rate coefficient became essentially the same as that of the CSDM one.

The comparison between the WP and CSDM results for R1 clearly indicates that the semiclassical method is reliable in treating nonadiabatic dynamics in the current system. This validation is particularly important because the intersystem crossing probability is quite small for this light system.

III.C. Excitation of N(⁴S)

Figure 6 displays calculated $J=0$ quantum excitation probabilities for N(⁴S) (R-1). In panels (a) and (b), the excitation probabilities with the N₂ in the $v_i=0$ initial state are displayed. Consistent with the quenching process, the WP results for both the ²A'' and ²A' states feature small and highly oscillatory probabilities. Both exhibit a threshold near 2.5 eV, clearly associated with the N(²D)-N(⁴S) energy gap. In panels (c) and (d), the effect of vibrational excitation of the N₂ collision partner is examined. The vibrational excitation does not significantly change the excitation probabilities, consistent with the observation that the crossing seams between the doublet and quartet PESs are largely along the N-N vibrational coordinate. However, the N₂($v_i=1$) probabilities do shift the threshold to lower energies, suggesting some energy transfer

from the vibrational coordinate to the reaction coordinate.

The CSDM results are also included in **Figure 6** for comparison. Because of the large endoergicity of R-1, there is substantial ZPE leakage from the N_2 collisional partner in such classical trajectory-based simulations. As a result, there is significant CSDM probability below the threshold, as shown in the figure. This problem can be mitigated by various correction schemes. The simplest approach is to remove trajectories that emerge on the excited doublet asymptote with the N_2 vibrational energy below its ZPE.⁶⁰ This so-called hard-ZPE scheme is shown to underestimate the WP results, because most trajectories are only slightly below the ZPE. However, the agreement with the WP results improves for $N_2(v_i=1)$, as the increased initial vibrational energy prevented most trajectories from violating the ZPE of the N_2 product. This is particularly significant concerning the location of the threshold. A more reasonable scheme to mitigate the ZPE problem is to use Gaussian weighting in binning the N_2 product vibrational quantum number, as described in Sec. II. Indeed, this so-called GB method also improves the agreement with the WP results, as shown in **Figure 6**. The ZPE correction is necessary to achieve agreement with the WP results for this endoergic process.

Figure 7 displays the calculated rate coefficients of R-1, R2a, and R2b obtained using the CSDM method with the GB correction. It is clear that the rate coefficient for the adiabatic exchange reaction (R2b) is approximately two orders of magnitude larger than the other two nonadiabatic processes, which have similar rate coefficients. The

small rate coefficients for R-1 and R2a can be readily understood as a direct result of the weak spin-orbit coupling between the doublet and quartet states in this system. The calculated R2b rate coefficient has an activation energy of ~ 2.77 eV, which can be attributed to the barrier for the adiabatic exchange channel on the quartet PES. The activation energy for both the R-1 and R2a reactions is around 2.5 eV, which is largely due to the energy gap between the $N(^4S)$ and $N(^2D)$ species. The small rate coefficients for these two spin-forbidden processes have also been seen in our recent investigation of the excitation of $C(^3P)$ to $C(^1D)$ by collisions with N_2 .⁴⁶ There is no experimental data to compare with, as no such measurements have so far been reported.

IV. Conclusions

In this work, we have investigated the nonadiabatic quenching of $N(^2D)$ and excitation of $N(^4S)$ through collisions with N_2 molecules. The spin-forbidden dynamics were investigated using a quantum WP method and the semi-classical CSDM approach, on recently developed PESs and spin-orbit couplings. For the quenching process, the agreement between the WP and CSDM results for $J=0$ is reasonable, even when the nonadiabatic transition is a small probability event. This comparison suggested that the semi-classical treatment is reliable for the spin-flipping process. The CSDM rate coefficients are in satisfactory agreement with available experimental data, further validating its accuracy. The same methods were then used to investigate the excitation process and the rate coefficients were calculated. Our results indicate that the CSDM treatment needs be corrected for ZPE violation in this highly endoergic process, and the

GB method provides an excellent approximation of the WP results. Overall, the hyperthermal collision between $N(^4S)$ and N_2 is dominated by the exchange channel on the quartet PES, while the nonadiabatic exchanging and non-exchanging excitation to $N(^2D)$ have rate coefficients that are two orders of magnitude smaller than the adiabatic process. These results are expected to provide guidance for modeling of kinetics of various chemical environments under extreme conditions.

Acknowledgments: This work was supported by a MURI grant from ONR (N00014-22-1-2661) and the calculations were performed at the Center for Advanced Research Computing (CARC) at UNM. BRLG thanks Conselho Nacional de Desenvolvimento Científico e Tecnológico (CNPq, Grant 311508/2021-9) and AJCV acknowledges support from Foundation for Science and Technology, Portugal, and Coimbra Chemistry Centre, Portugal, through Project UID/QUI/00313/2019. HG thanks Tim Minton and Iain Boyd for useful discussions.

References:

1. R. J. Donovan and D. Husain, *Chem. Rev.*, 1970, **70**, 489-516.
2. K. Schofield, *J. Phys. Chem. Ref. Data*, 1979, **8**, 723-798.
3. P. Casavecchia, N. Balucani, M. Alagia, L. Cartechini and G. G. Volpi, *Acc. Chem. Res.*, 1999, **32**, 503-511.
4. R. W. Schunk and A. F. Nagy, *Ionospheres: Physics, Plasma Physics and Chemistry*, Cambridge University Press, Cambridge, UK, 2009.

5. J. A. Miller and C. T. Bowman, *Prog. Energy Combust. Sci.*, 1989, **15**, 287.
6. K. S. Prata, T. E. Schwartzenruber and T. K. Minton, *AIAA J.*, 2021, **60**, 627-640.
7. I. D. Boyd and E. Josyula, *J. Thermophys. Heat Transfer*, 2021, **35**, 484-493.
8. G. Black, T. G. Slinger, G. A. St. John and R. A. Young, *J. Chem. Phys.*, 1969, **51**, 116-121.
9. C. L. Lin and F. Kaufman, *J. Chem. Phys.*, 1971, **55**, 3760-3770.
10. D. Husain, L. J. Kirsch and J. R. Wiesenfeld, *Faraday Disc. Chem. Soc.*, 1972, **53**, 201-210.
11. D. Husain, S. K. Mitra and A. N. Young, *J. Chem. Soc., Faraday Trans. 2*, 1974, **70**, 1721-1731.
12. T. G. Slinger and G. Black, *J. Chem. Phys.*, 1976, **64**, 4442-4444.
13. K.-i. Sugawara, Y.-i. Ishikawa and S. Sato, *Bull. Chem. Soc. Japan*, 1980, **53**, 3159-3164.
14. T. Suzuki, Y. Shihira, T. Sato, H. Umemoto and S. Tsunashima, *J. Chem. Soc., Faraday Trans. 2*, 1993, **89**, 995-999.
15. J. T. Herron, *J. Phys. Chem. Ref. Data*, 1999, **28**, 1453-1483.
16. J. M. L. Martin, J. P. François and R. Gijbels, *J. Chem. Phys.*, 1989, **90**, 6469-6485.
17. J. Wasilewski, *J. Chem. Phys.*, 1996, **105**, 10969-10982.
18. P. Zhang, K. Morokuma and A. M. Wodtke, *J. Chem. Phys.*, 2004, **122**, 014106.
19. P. C. Samartzis and A. M. Wodtke, *Int. Rev. Phys. Chem.*, 2006, **25**, 527-552.
20. A. Lagana, E. Garcia and L. Ciccarelli, *J. Phys. Chem.*, 1987, **91**, 312-314.
21. E. Garcia, A. Saracibar, A. Laganà and D. Skouteris, *J. Phys. Chem. A*, 2007, **111**,

- 10362-10368.
22. E. Garcia, A. Saracibar, S. Gómez-Carrasco and A. Laganà, *Phys. Chem. Chem. Phys.*, 2008, **10**, 2552-2558.
23. D. Wang, J. R. Stallcop, W. M. Huo, C. E. Dateo, D. W. Schwenke and H. Partridge, *J. Chem. Phys.*, 2003, **118**, 2186-2189.
24. D. Babikov, P. Zhang and K. Morokuma, *J. Chem. Phys.*, 2004, **121**, 6743-6749.
25. Z. Wang, I. S. K. Kerkines, K. Morokuma and P. Zhang, *J. Chem. Phys.*, 2009, **130**, 044313.
26. B. R. L. Galvão and A. J. C. Varandas, *J. Phys. Chem. A*, 2009, **113**, 14424-14430.
27. B. R. L. Galvão and A. J. C. Varandas, *J. Phys. Chem. A*, 2011, **115**, 12390-12398.
28. B. R. L. Galvão, P. J. S. B. Caridade and A. J. C. Varandas, *J. Chem. Phys.*, 2012, **137**, 22A515.
29. D. Wang, W. M. Huo, C. E. Dateo, D. W. Schwenke and J. R. Stallcop, *J. Chem. Phys.*, 2004, **120**, 6041-6050.
30. S. Rampino, D. Skouteris, A. Laganà, E. Garcia and A. Saracibar, *Phys. Chem. Chem. Phys.*, 2009, **11**, 1752-1757.
31. P. J. S. B. Caridade, B. R. L. Galvão and A. J. C. Varandas, *J. Phys. Chem. A*, 2010, **114**, 6063-6070.
32. M. Panesi, R. L. Jaffe, D. W. Schwenke and T. E. Magin, *J. Chem. Phys.*, 2013, **138**, 044312.
33. B. R. L. Galvão, A. J. C. Varandas, J. P. Braga and J. C. Belchior, *Chem. Phys. Lett.*, 2013, **577**, 27-31.

34. S. Korutla, D. Koner, A. J. C. Varandas and R. R. Tammineni, *J. Phys. Chem. A*, 2021, **125**, 5650-5660.
35. S. Mahapatra, *Int. Rev. Phys. Chem.*, 2004, **23**, 483-512.
36. T.-S. Chu, Y. Zhang and K.-L. Han, *Int. Rev. Phys. Chem.*, 2006, **25**, 201-235.
37. D. H. Zhang and H. Guo, *Annu. Rev. Phys. Chem.*, 2016, **67**, 135-158.
38. J. C. Tully, *J. Chem. Phys.*, 2012, **137**, 22A301.
39. J. C. Tully, *J. Chem. Phys.*, 1990, **93**, 1061-1071.
40. J. E. Subotnik, A. Jain, B. Landry, A. Petit, W. Ouyang and N. Bellonzi, *Annu. Rev. Phys. Chem.*, 2016, **67**, 387-417.
41. A. W. Jasper, C. Zhu, S. Nangia and D. G. Truhlar, *Faraday Discuss.*, 2004, **127**, 1-22.
42. M. Persico and G. Granucci, *Theo. Chem. Acc.*, 2014, **133**, 1526.
43. L. Wang, A. Akimov and O. V. Prezhdo, *J. Phys. Chem. Lett.*, 2016, **7**, 2100-2112.
44. C. Zhu, S. Nangia, A. W. Jasper and D. G. Truhlar, *J. Chem. Phys.*, 2004, **121**, 7658-7670.
45. A. W. Jasper, S. Nangia, C. Zhu and D. G. Truhlar, *Acc. Chem. Res.*, 2006, **39**, 101-108.
46. D. Lu and H. Guo, *J. Phys. Chem. A*, 2023, **127**, 3190-3199.
47. B. R. L. Galvão, A. J. C. Varandas, J. P. Braga and J. C. Belchior, *J. Phys. Chem. Lett.*, 2013, **4**, 2292-2297.
48. B. R. L. Galvão, J. P. Braga, J. C. Belchior and A. J. C. Varandas, *J. Chem. Theo. Comput.*, 2014, **10**, 1872-1877.
49. S. A. Lahankar, J. Zhang, T. K. Minton, H. Guo and G. Lendvay, *J. Phys. Chem. A*,

- 2016, **120**, 5348-5359.
50. A. Caracciolo, J. Zhang, S. A. Lahankar and T. K. Minton, *J. Phys. Chem. A*, 2022, **126**, 2091–2102.
51. D. Lu, D. G. Truhlar and H. Guo, *J. Phys. Chem. A*, 2022, **126**, 4277-4285.
52. D. Lu, R. Urzúa-Leiva, O. Denis-Alpizar and H. Guo, *J. Phys. Chem. A*, 2023, **127**, 2839-2845.
53. H. Guo, in *Theory of Chemical Reaction Dynamics*, eds. A. Lagana and G. Lendvay, Kluwer, Dordrecht2004, pp. 217-229.
54. R. Chen and H. Guo, *J. Chem. Phys.*, 1996, **105**, 3569-3578.
55. H. Tal-Ezer and R. Kosloff, *J. Chem. Phys.*, 1984, **81**, 3967-3971.
56. R. Kosloff, *Annu. Rev. Phys. Chem.*, 1994, **45**, 145.
57. Z. Sun, S.-Y. Lee, H. Guo and D. H. Zhang, *J. Chem. Phys.*, 2009, **130**, 174102.
58. J. M. Bowman, *J. Phys. Chem.*, 1991, **95**, 4960-4968.
59. J. Zheng, Z.-H. Li, A. W. Jasper, D. A. Bonhommeau, R. Valero, R. Meana-Pañeda, S. L. Mielke, L. Zhang and D. G. Truhlar, University of Minnesota, Minneapolis2019.
60. Y. Guo, D. L. Thompson and T. D. Sewell, *J. Chem. Phys.*, 1996, **104**, 576-582.
61. L. Bonnet and J.-C. Rayez, *Chem. Phys. Lett.*, 2004, **397**, 106-109.
62. A. J. C. Varandas, *Chem. Phys. Lett.*, 2007, **439**, 386-392.
63. L. Bonnet and J. Espinosa-Garcia, *J. Chem. Phys.*, 2010, **133**, 164108.
64. H.-J. Werner and P. J. Knowles, *J. Chem. Phys.*, 1988, **89**, 5803-5814.
65. P. J. Knowles and H.-J. Werner, *Chem. Phys. Lett.*, 1988, **145**, 514-522.
66. J. D. Watts, J. Gauss and R. J. Bartlett, *J. Chem. Phys.*, 1993, **98**, 8718-8733.

67. A. J. C. Varandas, *J. Chem. Phys.*, 2007, **126**.
68. T. H. Dunning, *J. Chem. Phys.*, 1989, **90**, 1007-1023.
69. R. A. Kendall, T. H. Dunning and R. J. Harrison, *J. Chem. Phys.*, 1992, **96**, 6796-6806.
70. A. J. C. Varandas, *Adv. Chem. Phys.*, 1988, **74**, 255-338.

Table 1. Numerical parameters used in the quantum WP calculations. Atomic units are used unless stated otherwise.

Parameter	Value
Grid/basis range and sizes	$R \in (0.01, 18)$, ($N_R=550$) $r \in (0.6, 6.8)$, ($N_r=110$) $j \in 0 - j_{\max} = 130$
Initial wave packet	$R_i=12$ and $\tau=0.13$, $k_i=(2E_0\mu_R)^{1/2}$ with $E_0=0.4$ (R1)/2.6 (R-1) eV
Propagation steps	100 000

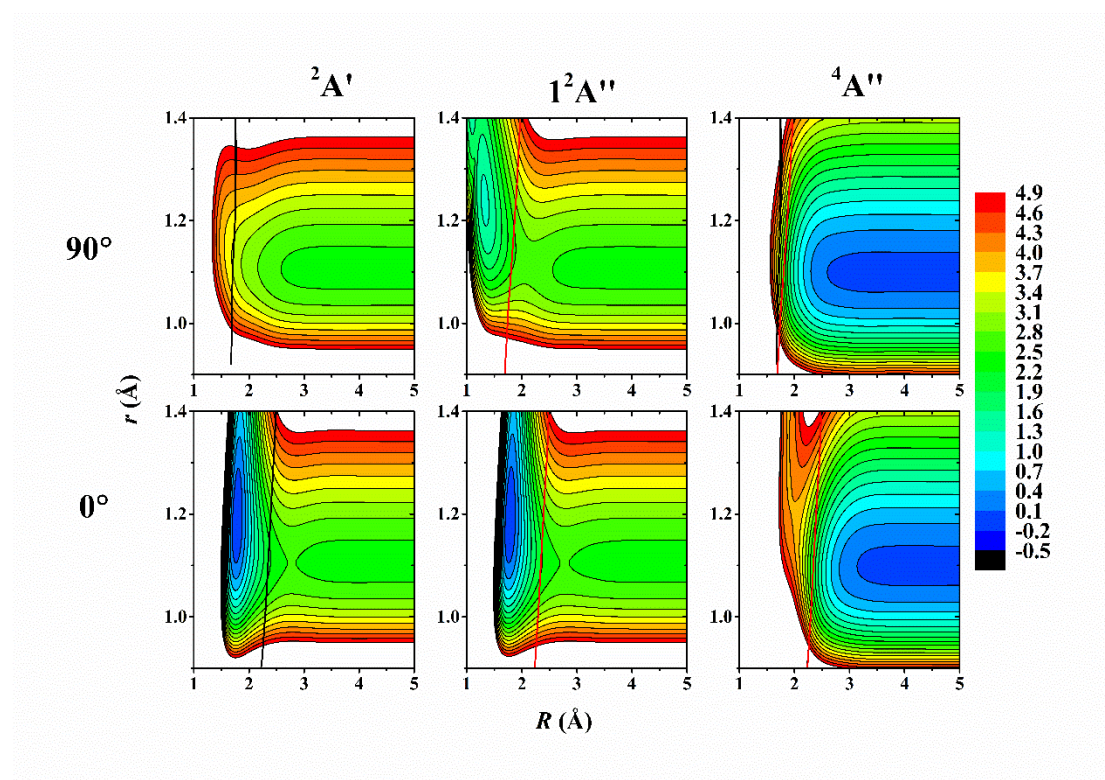


Figure 1. Contour plots of the diabatic PESs at two different angles ($\theta=0^\circ$ and 90°). The crossing seam between the quartet and doublet PESs is illustrated by the black

and red solid lines. The energy is given in eV relative to the $N(^4S) + N_2$ asymptote.

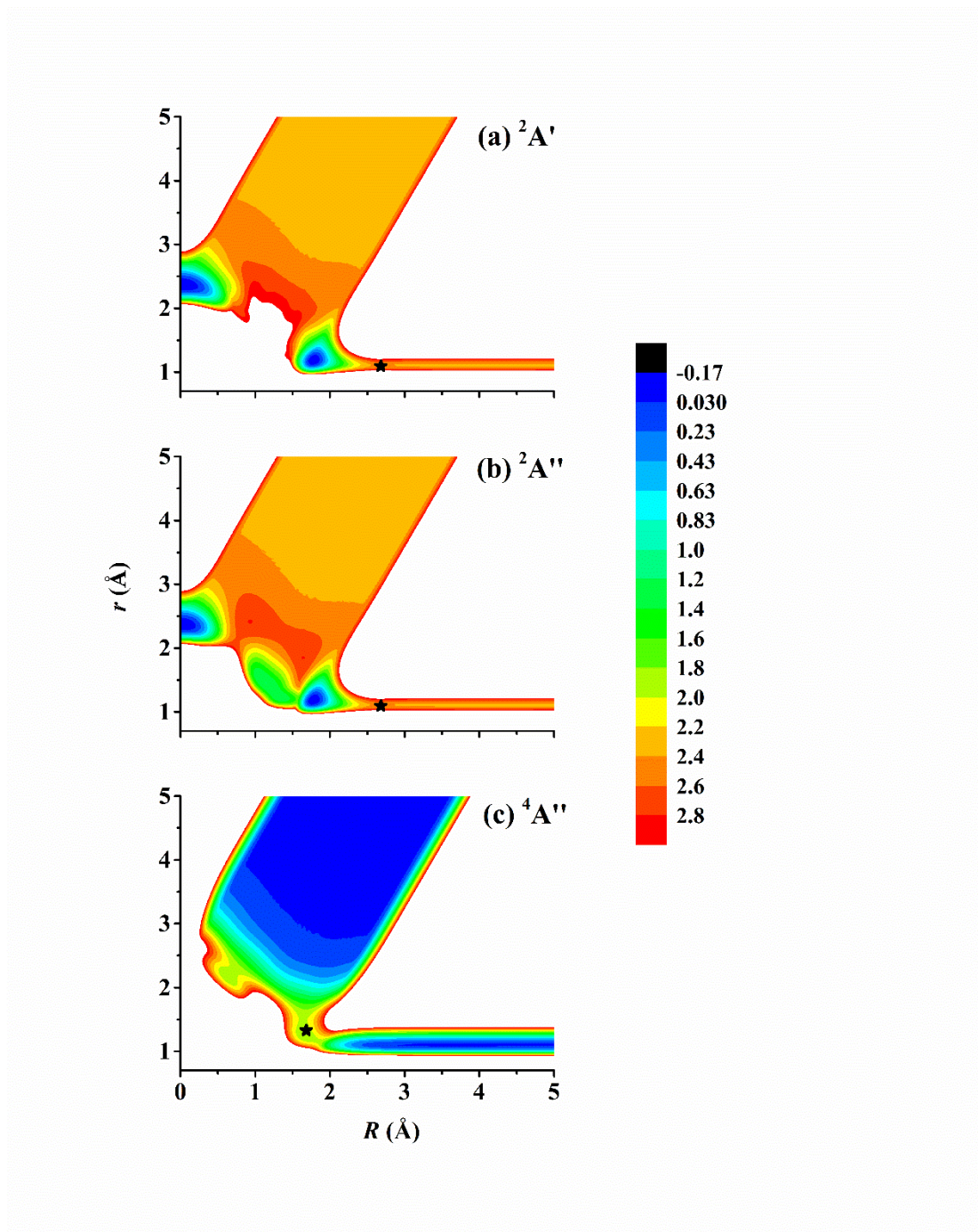


Figure 2. Contour plots of the diabatic PESs along the radial Jacobi coordinates with θ optimized. The stars represent the location of the classical barrier on each PES. The energy is given in eV relative to the $N(^4S) + N_2$ asymptote.

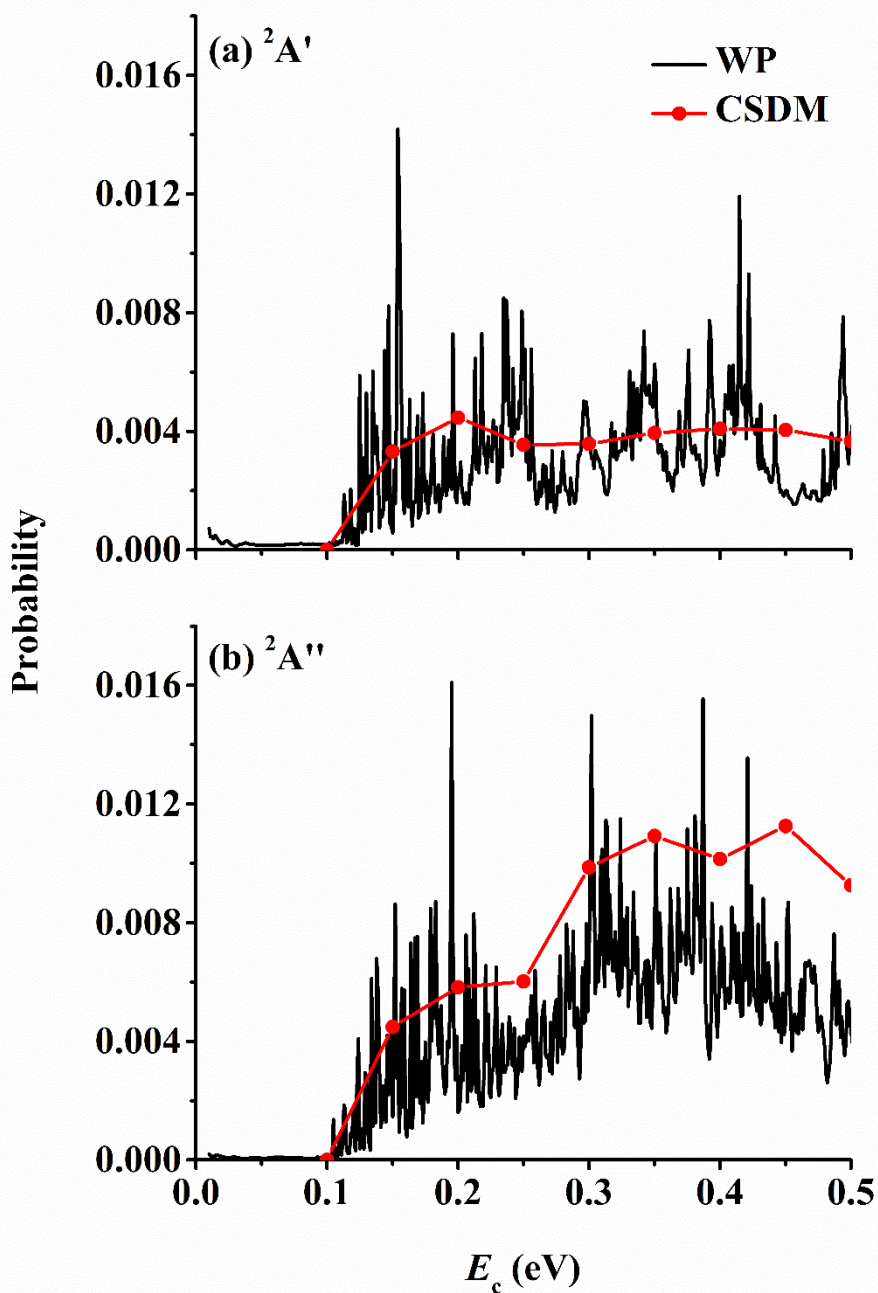


Figure 3. Comparison of $J=0$ reaction probabilities for $\text{N}(^2\text{D}) + \text{N}_2(v_i=0, j_i=0) \rightarrow \text{N}(^4\text{S}) + \text{N}_2(v_f, j_f)$ calculated using WP and CSDM methods, as a function of collision energy.

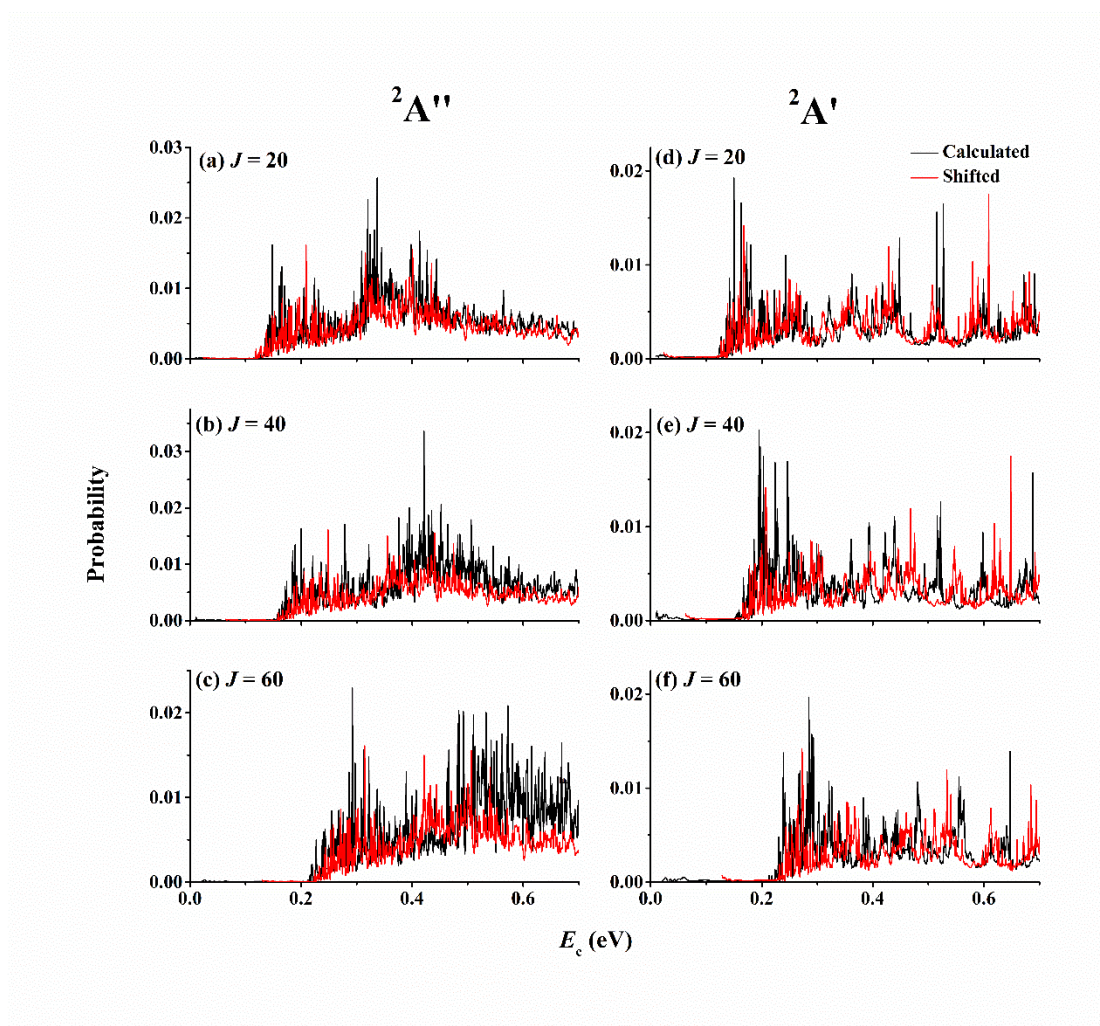


Figure 4. Comparisons of several explicitly calculated WP transition probabilities for $\text{N}(^2\text{D}) + \text{N}_2 \rightarrow \text{N}(^4\text{S}) + \text{N}_2$ at several partial waves with the J -shifted results.

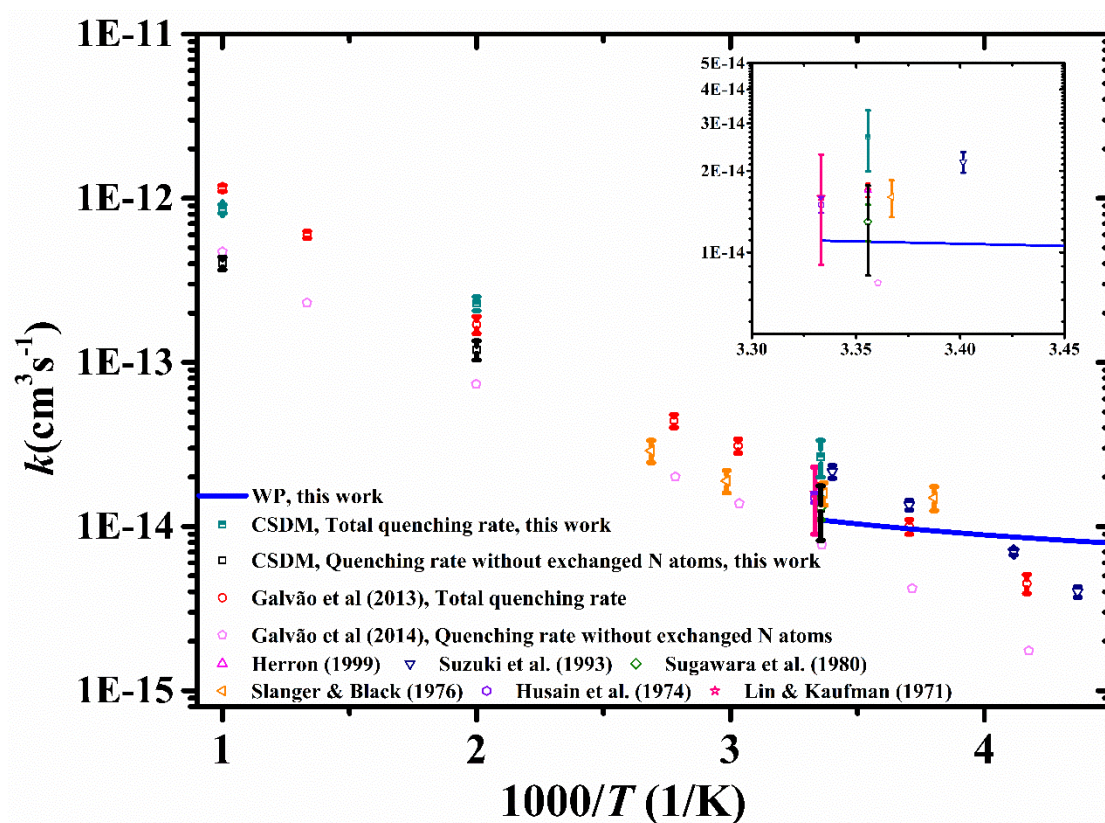


Figure 5. Comparisons of the rate constants for $\text{N}(^2\text{D}) + \text{N}_2 \rightarrow \text{N}(^4\text{S}) + \text{N}_2$ calculated by CSDM (square) and WP (blue line) methods, The CSDM results are thermal rate coefficients while the QD are vibrational state specified ($v_i=0$) rate coefficients. The previous theoretical^{47, 48} and experimental results^{9, 11-15} are also included for comparison.

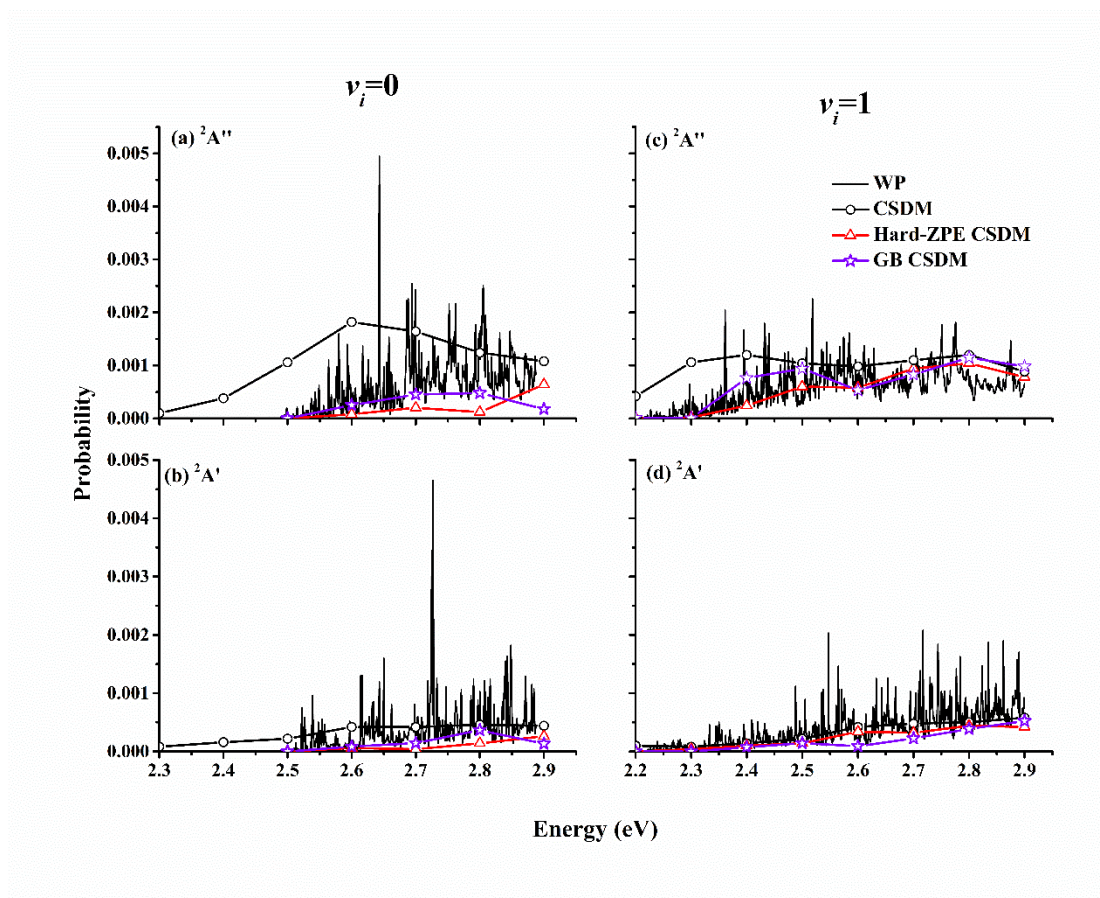


Figure 6. Comparison of $J=0$ reaction probabilities for $\text{N}(^4\text{S}) + \text{N}_2(v_i=0/1, j_i=0) \rightarrow \text{N}(^2\text{D}) + \text{N}_2(v_f, j_f)$ calculated using WP and CSDM methods, as a function of collision energy. The ZPE-corrected CSDM results based on the hard-ZPE and GB scheme are also included in for comparison.

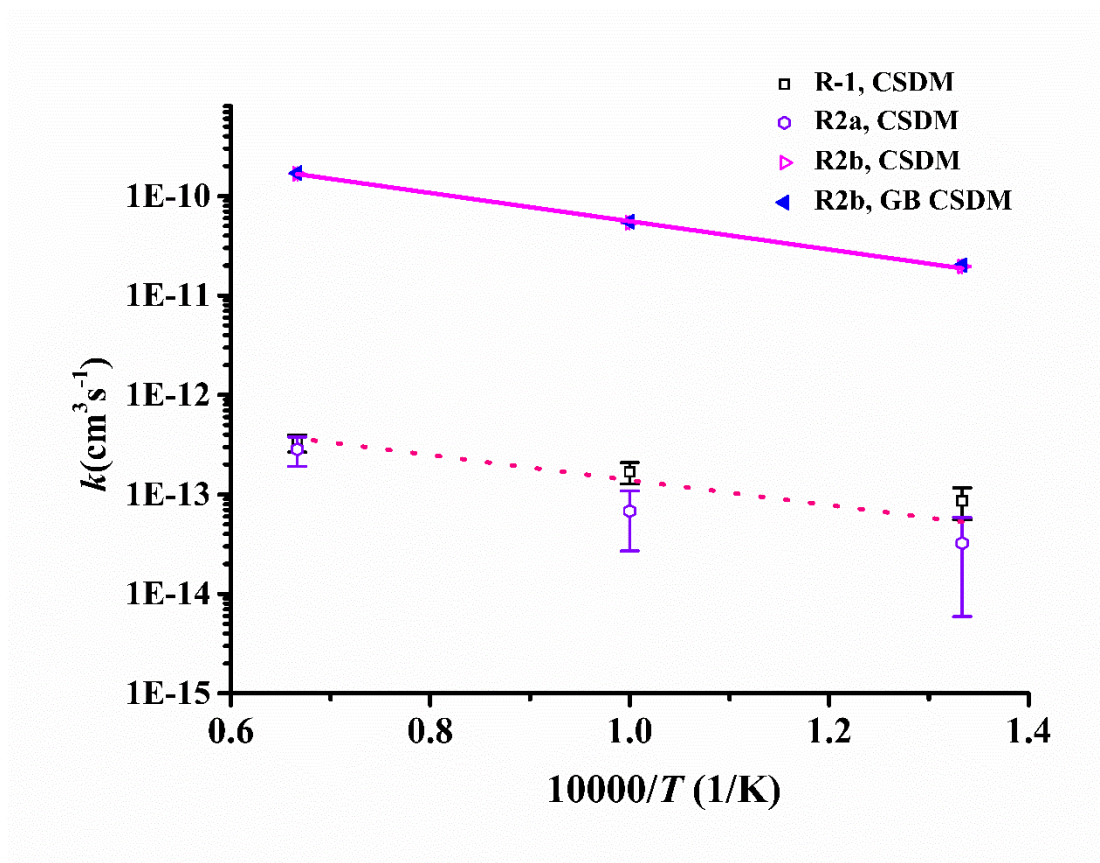


Figure 7. Comparisons of the rate coefficients for excitation (R-1), exchange-excitation (R2a), and exchange (R2b) calculated by the CSDM method. The GB methods also used for R2a. The data are fit to lines from which the activation energy is extracted according to the Arrhenius equation. For R-1 and R2a, the errors are too large to extract an accurate fit, so that the dashed line for an activation energy of 2.5 eV is used to guide the eye.